Microwave Kinetic Inductance Detector Made of Molecular Beam Epitaxy (MBE)-Grown MgB2 Film

Ariel Roitman, Corentin Pfaff, Thomas Hauet, Avner Shaulov, Yosef Yeshurun

nanomaterials

MDPI

Article

Microwave Kinetic Inductance Detector Made of Molecular Beam Epitaxy (MBE)-Grown MgB2 Film

Ariel Roitman [1,2,*], Corentin Pfaff [3], Thomas Hauet [3], Avner Shaulov [1,2] and Yosef Yeshurun [1,2,*]

[1] Institute of Superconductivity, Department of Physics, Bar-Ilan University, Ramat-Gan 5290002, Israel; shauloa@mail.biu.ac.il
[2] Institute of Nanotechnology, Bar-Ilan University, Ramat-Gan 5290002, Israel
[3] Institut Jean Lamour, Université de Lorraine, Centre National de la Recherche Scientifique (CNRS), F-54000 Nancy, France; corentin.pfaff@univ-lorraine.fr (C.P.); thomas.hauet@univ-lorraine.fr (T.H.)
* Correspondence: roitmaa@biu.ac.il (A.R.); yeshurun@mail.biu.ac.il (Y.Y.)

Abstract: We present a MgB_2-based Microwave Kinetic Inductance Detector (MKID) featuring a quality factor $Q_i \sim 10^5$ and noise equivalent power NEP ~ 10^{-14} W/$\sqrt{\text{Hz}}$ at 2 K. In comparison to YBCO-based MKIDs, the MgB_2 detector shows greater sensitivity to both temperature and magnetic field, a result of its two-gap nature and relatively low critical H_{c2} field. Our data indicate that MgB_2 is more advantageous for MKID applications at temperatures lower than 3 K.

Keywords: MBE-grown superconductors; kinetic inductance detector; MgB_2

1. Introduction

Microwave Kinetic Inductance Detectors (MKIDs) represent a state-of-the-art technology in the field of superconducting photon detectors, offering exceptional sensitivity and multiplexing capabilities [1–3]. These detectors are fabricated from superconducting films lithographically patterned into a microwave LC resonance circuit. Incident photons with sufficient energy break Cooper pairs inside the superconductor, causing a change in its kinetic inductance which is observed as a shift in the resonance frequency.

Traditionally, low-T_c superconductors, such as Al [4] and Nb [5], have been employed in the fabrication of MKIDs, owing to their well-understood superconducting properties and relatively straightforward fabrication processes. There have been limited reports of MKIDs made out of superconductors with relatively high T_c, such as $YB_2Cu_3O_{7-\delta}$ (YBCO) and MgB_2 [6]. The motivation for exploring these materials for application in MKIDs is their potential for operation at relatively high temperatures, reducing the complexity and cost of cooling systems. An MKID made of YBCO was reported by Sato et al. [7], featuring a relatively low-quality factor of $Q_i \sim 3000$ and relatively high noise equivalent power (NEP) of $\sim 10^{-9}$ W/$\sqrt{\text{Hz}}$ at 13 K. Roitman et al. [8] found better Q_i and NEP, with values of 2.5×10^4 and $\sim 10^{-12}$ W/$\sqrt{\text{Hz}}$ at 10 K, respectively, using thinner YBCO films and an improved fabrication technique. MgB_2 with a T_c of around 39 K [9] offers some advantages over YBCO, such as a simple crystal structure, being composed of two abundant, low-cost elements, as well as mechanical robustness, making it easier to handle compared to the more brittle YBCO. Most of the publications on MgB_2 relevant to its application in MKIDs [6,10–13] focus on studying temperature and field dependence of their resonance frequency, f_r, and the quality factor, Q_i. For example, Yang et al. [10] reported on lumped-element KIDs made of MgB_2 thin films fabricated by hybrid physical–chemical vapor deposition (HPCVD) and found a high loaded quality factor, $Q_L \sim 30{,}000$ at 7.5 K, comparable to that of lower-operating-temperature lumped-element KIDs made from superconductors such as Al and Nb.

The effect of the two gaps characterizing MgB_2 on the microwave properties of this material was investigated by Ghigo et al. [11]. They measured the complex impedance of

check for updates

Citation: Roitman, A.; Pfaff, C.; Hauet, T.; Shaulov, A.; Yeshurun, Y. Microwave Kinetic Inductance Detector Made of Molecular Beam Epitaxy (MBE)-Grown MgB2 Film. *Nanomaterials* **2024**, *14*, 1731. https://doi.org/10.3390/nano14211731

Academic Editors: Filippo Giubileo and Ming-Yu Li

Received: 19 September 2024
Revised: 14 October 2024
Accepted: 28 October 2024
Published: 29 October 2024

polycrystalline MgB_2 films using a coplanar waveguide resonator technique. The Q_i for their device at 5 K was ~60,000. They concluded that the temperature dependence of the penetration depth can be accounted for by an effective mean energy gap, in agreement with the predictions of Kogan [14]. Data on MgB_2 MKIDs as a photon detector, namely, responsivity and noise equivalent power, are scarce.

In this paper, we report on an MKID made of molecular beam epitaxy (MBE)-grown MgB_2 [15–18] and characterize it as a photon detector. The aim of using a relatively clean MBE-grown MgB_2 was to obtain a better efficiency of Cooper pairs breaking and thus a better responsivity and lower NEP. The performance of this MKID is compared with that of an MKID made of 50 nm thick YBCO with a T_c of around 84 K [8]. Although these MKIDs show qualitatively similar temperatures and magnetic field dependences of f_r and Q_i, quantitatively, they are very different. The MgB_2-based detector exhibits a much stronger decrease in the resonance frequency and the quality factor with increasing temperature or magnetic field. The strong temperature and field dependence in MgB_2 are ascribed below to its two-gap nature and relatively lower second critical field H_{c2}, respectively.

2. Materials and Methods

Our MgB_2 MKID consisted of a rewound spiral $\lambda/2$ coplanar waveguide resonator coupled to a 50 Ohm transmission line, as shown in Figure 1. The device was lithographically patterned on a single-crystal 33 nm thick MgB_2 film deposited by molecular beam epitaxy (MBE) under ultrahigh vacuum on sapphire (0001) single-crystal substrate, as described in Ref. [18]. A 5 nm thick epitaxial MgO (111) buffer layer was deposited prior to MgB_2 in order to allow single-crystal growth of MgB_2. A 5 nm thick capping layer of gold protected the MgB_2 layer against oxidation. The temperature dependence of the film resistance indicated a sharp transition at $T_c = 24.3$ K.

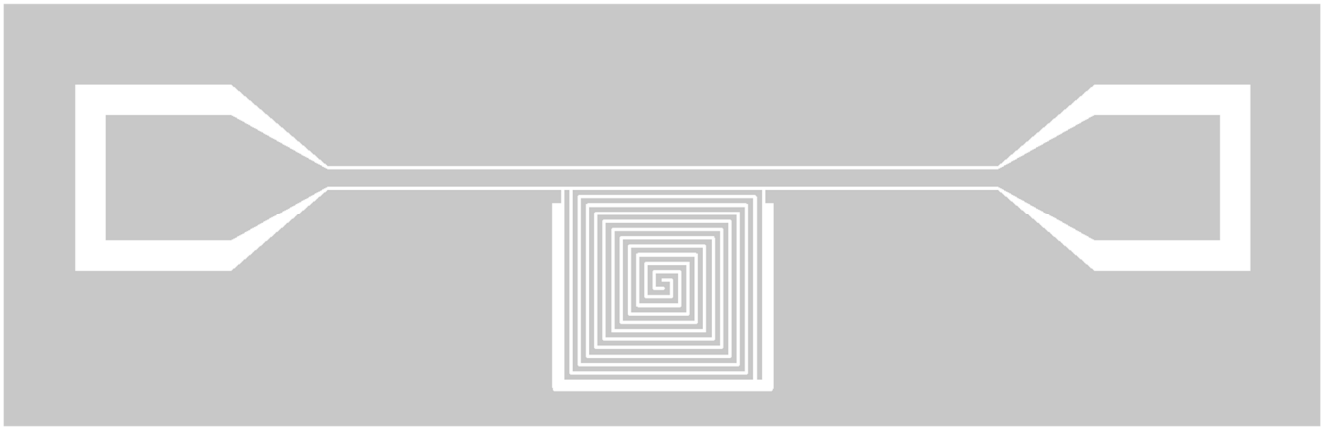

Figure 1. Schematic of the MgB_2 MKID. In white: bare substrate. In gray: superconductor. The resonator linewidth is 10 μm with 10 μm between lines.

The patterning process was conducted as follows. The film was coated with AZ1518 photoresist using a spin coater, followed by hot plate baking at 100 °C. Lithography was performed using a Maskless Laser Aligner (MLA150) by Heidelberg Instruments (Heidelberg, Germany) after dose calibration, followed by a photoresist development in AZ351b:H_2O 1:4 developer. The Ar milling process was conducted in 4 s pulses, with nitrogen gas cooling in between pulses to prevent heating of the photoresist. The resist was subsequently removed using acetone to prevent any adverse effects on the resonator.

The fabricated MKID was placed in a dedicated setup inserted into a Quantum Design (Pfungstadt, Germany) Physical Property Measurement System (PPMS). The resonance frequency, f_r, and the internal quality factor, $Q_i = \frac{Q_L}{[S_{21}(f_r)]}$, ($Q_L = \frac{f_r}{\Delta f_{3db}}$) [8], were measured using a Keysight (Santa Rosa, CA, USA) Vector Network Analyzer (VNA) connected to the detector through a combination of 20 and 30 dB attenuators at the output of the VNA and

a High Electron Mobility Transistor (HEMT) amplifier and Low-Noise Amplifier (LNA) at its input. The HEMT and the 30 dB attenuator were cooled to ~5 K, while the 20 dB attenuator and the LNA were at room temperature. For the NEP measurements, the MKID was irradiated with 1064 nm light generated by an Yttrium Aluminum Garnet (YAG) laser and delivered by an optical fiber. The end of the optical fiber was positioned ~4 mm from the detector.

A magnetic field was applied perpendicular to the detector using the 9 Tesla magnet of the PPMS. In a zero-field-cooled (ZFC) procedure, the device was cooled in zero magnetic field, and then the magnetic field was changed in the superconducting phase. In the field-cooled (FC) procedure, the magnetic field was applied in the normal phase, and then the device was cooled down; the field remained unchanged in the superconducting phase.

3. Results

Figure 2 presents the temperature dependence of the resonance frequency, f_r, measured in zero magnetic field. As expected, f_r decreases with increasing temperature; however, it had a much higher rate compared to YBCO, as demonstrated in the inset in the figure, where $f_r(T)/f_r(0)$ is plotted versus T/T_c. As discussed below, the temperature dependence of f_r in MgB_2 reflects the two-gap nature of this material.

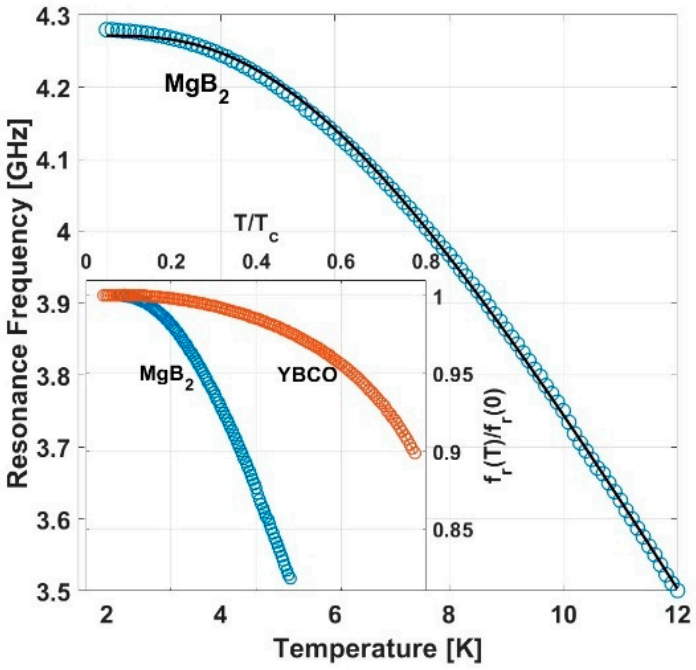

Figure 2. Temperature dependence of the resonance frequency, f_r, in zero magnetic field (main frame) for MgB_2 resonator. Solid line is calculated using Equation (4). Inset: comparison of $f_r(T)/f_r(0)$ vs. T/T_c in MgB_2 and YBCO. The data for YBCO are based on Ref. [8].

The temperature dependence of the internal quality factor, Q_i, measured in zero magnetic field is shown in Figure 3. Far below T_c, a high value of Q_i, of order 10^5, is achieved; however, it rapidly deteriorates as T_c is approached. The inset in Figure 3 compares the behavior of Q_i vs. T/T_c in MgB_2 and YBCO. Similar to the behavior of f_r, Q_i in YBCO also decreases more moderately with increasing temperature compared to MgB_2. Interestingly, while Q_i in YBCO saturates at low temperatures, in MgB_2 it continues to increase as temperature decreases, reaching values well above those of YBCO.

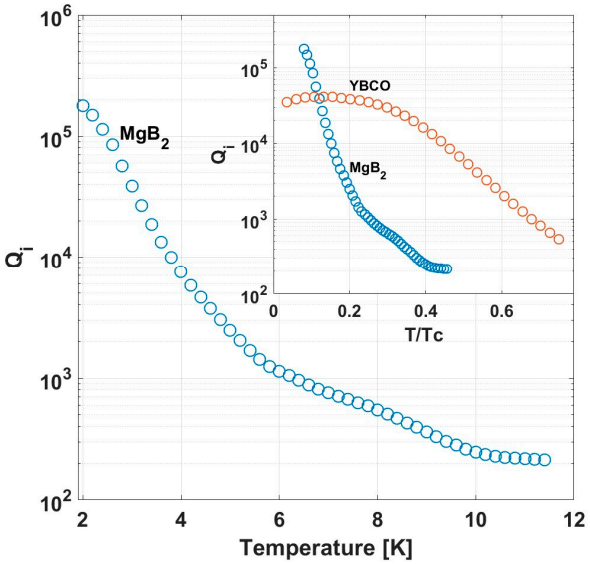

Figure 3. Quality factor vs. temperature for MgB_2 in zero magnetic field (main frame). Inset: comparison of Q_i vs. T/T_c in MgB_2 and YBCO.

Figure 4 shows ZFC and FC measurements of the field dependence of f_r at 2.3 K with fields up to 0.12 T and down to −0.12 T and back to zero. Similar to the behavior previously observed in resonators made of other materials [8,19–23], MgB_2 also exhibits an initial sharp drop in f_r followed by an approximately linear drop with the field. Also, as previously observed, there is a substantial difference between the ZFC and FC measurements. The later shows approximately a linear decrease with the field in the entire field range in contrast to the relatively more complex ZFC data. While the qualitative behavior of f_r vs. H in MgB_2, mainly the linear decrease with field, is similar to that observed in resonators made of other materials, quantitively, it is very different. The inset in Figure 4 compares $f_r(H)/f_r(0)$ in resonators made of MgB_2 and YBCO at $T/T_c \cong 1/6$. Evidently, the two materials exhibit drastically different linear slopes, -9.6×10^{-1} and -8×10^{-3} 1/Tesla for MgB_2 and YBCO, respectively. In the discussion below, we relate this difference to the different second critical fields in these materials.

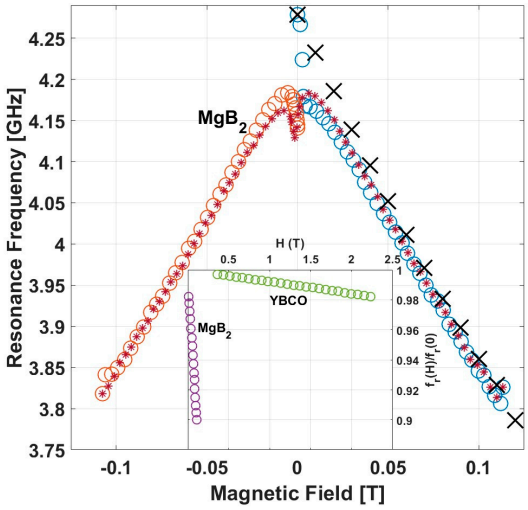

Figure 4. ZFC and FC measurements of the field dependence of f_r at 2.3 K of the MgB_2 resonator. In ZFC, the field was ramped up from 0 to 0.12 T (blue circles). It was then ramped down to −0.12 T (red stars) and back to 0 (orange circles). The FC data are denoted by black X's. Inset: Comparison of $f_r(H)/f_r(0)$ vs. magnetic field in MgB_2 and YBCO at $T/T_c \cong 1/6$.

A high sensitivity of Q_i to the magnetic field in the MgB_2 resonator is also exhibited in measurements of Q_i vs. H, as shown in the main frame of Figure 5; from a zero-field value of order 10^5, Q_i drops by more than an order of magnitude already at a field of ~0.01 T. As the field increases, it continues to drop moderately in a similar fashion, as observed in the YBCO resonator [8]. The inset in Figure 5 compares the losses due to the magnetic field, $1/Q_H = 1/Q_i(H) - 1/Q_i(0)$, in MgB_2 and YBCO resonators at $T/T_c \cong 1/6$. Evidently, the losses associated with the field are much more significant in MgB_2 as compared to YBCO.

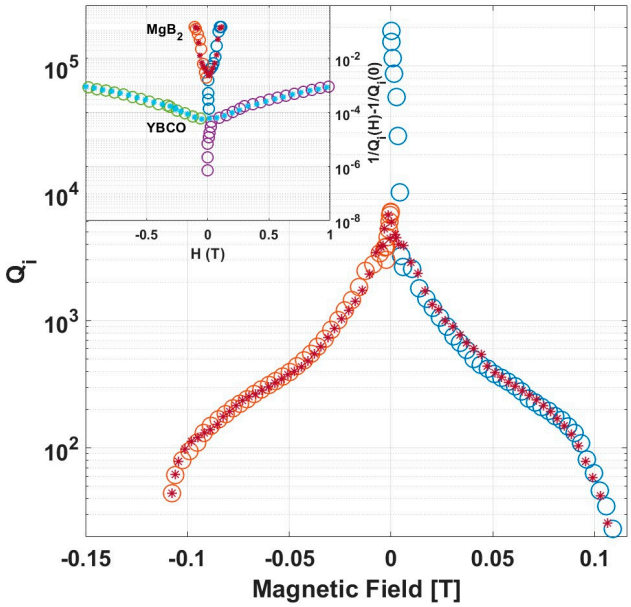

Figure 5. ZFC measurements of the field dependence of Q_i at 2.3 K. Color-coding is the same as in Figure 4. Inset: comparison of $\frac{1}{Q_H} = \frac{1}{Q_i(H)} - \frac{1}{Q_i(0)}$ vs. field in MgB_2 and YBCO at $T/T_c \cong 1/6$.

In addition to characterizing our MgB_2 MKID as a resonator, we also characterize it as a photon detector. In measurements of its responsivity and noise equivalent power, we follow the methodology outlined in Refs. [7,24]. The responsivity is calculated as $R_{es} = \Delta|S_{21}|^2/\Delta P$, where $\Delta|S_{21}|^2$ and ΔP denote the change in the power response and the absorbed power of the incident light, respectively. The responsivity was measured for two incident laser powers of 2.66 and 1.88 μW. The power response due to a 1 s pulse was 8 and 6 pW, respectively, yielding responsivities of 3.0 and 3.2 μW/W, respectively. The NEP is calculated as $\frac{P_n}{R_{es}\sqrt{\Delta f}}$, where P_n is the noise power in a bandwidth of Δf. The noise power at 2 K was about −140 dBm in a bandwidth (BW) of 10 kHz, yielding an NEP of about 3×10^{-14} and 3.2×10^{-14} W/$\sqrt{\text{Hz}}$, comparable to the NEP measured in NbN at 4.2 K [25]. To the best of our knowledge, this is the first reported NEP results that have been published on an MgB_2 MKID. The best NEP reported for an YBCO MKID is 10^{-12} W/$\sqrt{\text{Hz}}$, but this was measured at 10 K. We note that in evaluating the responsivity, we assumed that all the incident laser power is absorbed in the detector, leading to an underestimation of the responsivity; thus, the actual NEP may be even lower than estimated above.

4. Discussion

In the following, we show that the origin of the quantitative differences in the temperature and field dependence of the MgB_2 and YBCO resonators (see insets in Figures 2 and 3) are due to the two-gap nature of MgB_2 and its lower second critical field, respectively.

The resonance frequency of a half-wavelength superconducting microwave resonator is related to the London penetration depth, $\lambda_L(T)$, through the following equation [26]:

$$f_r = \frac{1}{2l\sqrt{\left(\frac{\mu_0\lambda_L^2}{A} + L_m\right)C}} \quad (1)$$

where A and C are the cross-section area of the resonator and its capacitance per unit length, respectively, $L_k = \mu_0\lambda_L^2/A$ and L_m are the kinetic and magnetic inductance per unit length, respectively, and l is the resonator length. As shown in Refs. [7,8], the temperature dependence of f_r in YBCO can be well described by the temperature dependence of λ_L as predicted by the two-fluid model:

$$\lambda_L = \lambda_0\left(1 - \left(\frac{T}{T_c}\right)^{\gamma}\right)^{-0.5}, \quad (2)$$

with the fitting parameter $\gamma = 2.6$. At an early stage of MgB_2 study, it was realized that Equation (2) cannot describe the measured temperature dependence of λ_L in this material [27,28].

Several authors developed new relations for $\lambda_L(T)$, taking into account the two-gap nature of MgB_2 [10,29,30]. The best fit to our data was obtained using the expression for $\lambda_L(T)$ given in Ref. [30]:

$$\lambda_L(T) = \lambda_L(0)\left(1 - 2a\sqrt{\frac{2\pi\Delta_\pi}{k_BT}}e^{-\frac{\Delta_\pi}{k_BT}} - 2(1-a)\sqrt{\frac{2\pi\Delta_\sigma}{k_BT}}e^{-\frac{\Delta_\sigma}{k_BT}}\right)^{-0.5} \quad (3)$$

where k_B is Boltzmann constant, $a = \frac{\lambda_\sigma^2}{\lambda_\pi^2+\lambda_\sigma^2}$, and Δ_π, Δ_σ and λ_π, λ_σ are the energy gaps and London penetration depths in the π and σ bands, respectively. Combining Equation (3) with Equation (1), one obtains

$$f_r(T) = f_r(0)\sqrt{1+\chi}\left(\left(1 - 2a\sqrt{\frac{2\pi\Delta_\pi}{k_BT}}e^{-\frac{\Delta_\pi}{k_BT}} - 2(1-a)\sqrt{\frac{2\pi\Delta_\sigma}{k_BT}}e^{-\frac{\Delta_\sigma}{k_BT}}\right)^{-1} + \chi\right)^{-0.5} \quad (4)$$

where $\chi = \frac{L_m}{L_k(0)}$, L_m and $L_k(0)$ are the magnetic and kinetic inductance of the resonators, respectively. Using SONNET, following the method described in Ref. [31], we found $\chi = 0.91$ for our MgB_2 resonator.

The solid curve in the main frame of Figure 2, calculated using Equation (4) and the parameter values shown in the second column of Table 1, shows a good fit to the data. These parameters are consistent with values reported in the literature for MgB_2 as listed in the third column of Table 1. The inset in Figure 2, comparing f_r vs. T/T_c in YBCO and MgB_2, clearly demonstrates that the two-gap model predicts a faster decrease in f_r with temperature as T_c is approached.

Table 1. Characteristic parameters of MgB_2 used for calculation of the solid line in Figure 2 compared with a range of reported values [30,32–37].

Parameters	Values Used in Calculation of f_r (Solid Line in Figure 3)	Range of Values Reported in the Literature
Δ_π	1.88 meV	1.5–3.5 meV
Δ_σ	6 meV	6–9 meV
λ_π	26 nm	20–40 nm
λ_σ	65 nm	40–70 nm

As mentioned above, the effect of the magnetic field on f_r, as described in Figure 4, appears qualitatively similar to results previously reported for resonators made of YBCO and other materials. All exhibit an initial sharp decrease in f_r in the ZFC data, which has been attributed to the effect of screening currents and a linear behavior thereafter, which has been attributed to the increase in the number of vortices within the resonator [8]. However, the slope df_r/dH of this linear decrease differ markedly between resonators made of different materials. This slope can be related to the second critical field, H_{c2}, of the material based on the following simplified analysis: The vortex density corresponding to H_{c2} transforms the entire sample to a normal state. Thus, assuming that the density of vortices is linear with field, the vortex density corresponding to field H transforms only a fraction of H/H_{c2} of the sample to a normal state, while the rest is in a superconducting state. Thus, the density of Cooper pairs, n_s, in field H is given by

$$n_s(H) = n_s(0)\left(1 - \frac{H}{Hc_2}\right), \tag{5}$$

yielding

$$L_k(H) = \frac{L_k(0)}{1 - H/H_{c2}}. \tag{6}$$

For $L_k(H) \gg L_m$, one obtains

$$f_r(H) = f_r(0)\left(1 - \frac{H}{H_{c2}}\right)^{\frac{1}{2}} \cong f_r(0)\left(1 - \frac{H}{2H_{c2}}\right) \tag{7}$$

for $H \ll H_{c2}$.

The range of the reported values of $H_{c2}(0)$ for MgB_2 and YBCO differ markedly (3–16 T [37–40] and 50–200 T [41–43], respectively). Thus, one would expect also markedly different slopes of f_r vs. H for resonators made of these two materials. This is demonstrated in the inset in Figure 4 in which $f_r(H)/f_r(0)$ is plotted versus H. The slopes of these straight lines (-9.6×10^{-1} and -8×10^{-3} 1/Tesla) yield H_{c2} values at $T/T_c = 1/6$ of 0.52 T and 63 T for MgB_2 and YBCO, respectively. For YBCO, this value of H_{c2} at $T/T_c = 1/6$ aligns with the values reported in the literature. However, the value of H_{c2} obtained for MgB_2 is lower than anticipated, a result that needs further investigation.

To explain the behavior of $Q_i(H)$, see Figure 5; we note that according to Equation (5), the lower H_{c2} in MgB_2 implies a rapid decrease in n_s with H. This gives rise to a rapid increase in the density of quasi-particles and thus to a rapid increase in the losses with field. This is demonstrated in the inset in Figure 5 in which the losses due to the field, $1/Q_H = 1/Q_i(H) - 1/Q_i(0)$, are plotted vs. field for MgB_2 and YBCO. Evidently, the losses in MgB_2 increase at a much higher rate than in YBCO, reflecting the higher rate of increase in quasi-particles in MgB_2 due to its smaller Hc_2.

In summary, exploring the application of MgB_2 MKIDs was motivated by their relatively high T_c, which could save the cost and complexity associated with low-temperature cooling systems. Comparing MKIDs made of MgB_2 and YBCO, we found that MgB_2 MKIDs are much more sensitive to temperature and external magnetic fields because of their two-gap nature and lower H_{c2}. This makes MgB_2 less attractive in MKID applications as compared to YBCO. However, at low temperatures, below 3 K, MgB_2 appears to be more advantageous due to its better Q_i and NEP. The high T_c and low Hc_2 make the MgB_2 resonator potentially applicable as a tunable resonator or a magnetic field sensing device that works at relatively high temperature [44–47].

Author Contributions: Conceptualization, A.R., A.S. and Y.Y.; Methodology, A.R., C.P., T.H., A.S. and Y.Y.; Formal analysis, A.R., A.S. and Y.Y.; Writing—original draft, A.R., A.S. and Y.Y.; Writing—review & editing, A.R., C.P., T.H., A.S. and Y.Y.; Supervision, T.H., A.S. and Y.Y. All authors have read and agreed to the published version of the manuscript.

Funding: This research received no external funding.

Data Availability Statement: Data is contained within the article.

Conflicts of Interest: The authors declare no conflict of interest.

References

1. Zmuidzinas, J. Superconducting Microresonators: Physics and Applications. *Annu. Rev. Condens. Matter Phys.* **2012**, *3*, 169. [CrossRef]
2. Mazin, B.A.; Young, B.; Cabrera, B.; Miller, A. Microwave Kinetic Inductance Detectors: The First Decade. *AIP Conf. Proc.* **2009**, *1185*, 135–142.
3. Ulbricht, G.; De Lucia, M.; Baldwin, E. Applications for Microwave Kinetic Induction Detectors in Advanced Instrumentation. *Appl. Sci.* **2021**, *11*, 2671. [CrossRef]
4. Grünhaupt, L.; Maleeva, N.; Skacel, S.T.; Calvo, M.; Levy-Bertrand, F.; Ustinov, A.V.; Rotzinger, H.; Monfardini, A.; Catelani, G.; Pop, I.M. Loss Mechanisms and Quasiparticle Dynamics in Superconducting Microwave Resonators Made of Thin-Film Granular Aluminum. *Phys. Rev. Lett.* **2018**, *121*, 117001. [CrossRef] [PubMed]
5. Gao, J.; Vale, L.R.; Mates, J.A.B.; Schmidt, D.R.; Hilton, G.C.; Irwin, K.D.; Mallet, F.; Castellanos-Beltran, M.A.; Lehnert, K.W.; Zmuidzinas, J.; et al. Strongly quadrature-dependent noise in superconducting microresonators measured at the vacuum-noise limit. *Appl. Phys. Lett.* **2011**, *98*, 232508. [CrossRef]
6. Mazin, B.A. H4.3 Superconducting Materials for Microwave Kinetic Inductance Detectors. In *Handbook of Superconductivity: Characterization and Applications*; CRC Press: Boca Raton, FL, USA, 2022.
7. Sato, K.; Ariyoshi, S.; Negishi, S.; Hashimoto, S.; Mikami, H.; Nakajima, K.; Tanaka, S. Evaluation of $YBa_2Cu_3O_{7-\delta}$ based microwave kinetic inductance detectors with rewound spiral resonators. *J. Phys. Conf. Ser.* **2018**, *1054*, 12053. [CrossRef]
8. Roitman, A.; Shaulov, A.; Yeshurun, Y. Characterization of $YBa_2Cu_3O_{7-\delta}$ coplanar resonator for microwave kinetic inductance detectors. *Supercond. Sci. Technol.* **2023**, *36*, 15002. [CrossRef]
9. Nagamatsu, J.; Nakagawa, N.; Muranaka, T.; Zenitani, Y.; Akimitsu, J. Superconductivity at 39 K in magnesium diboride. *Nature* **2001**, *413*, 63–64. [CrossRef]
10. Yang, C.; Niu, R.R.; Guo, Z.S.; Cai, X.W.; Chu, H.M.; Yang, K.; Wang, Y.; Feng, Q.R.; Gan, Z.Z. Lumped element kinetic inductance detectors based on two-gap MgB_2 thin films. *Appl. Phys. Lett.* **2018**, *112*, 22601. [CrossRef]
11. Ghigo, G. MgB2 Thin Films for Radiation Detectors Operating at Microwave Frequencies. *AIP Conf. Proc.* **2006**, *824*, 463–470.
12. Cherednichenko, S.; Acharya, N.; Novoselov, E.; Drakinskiy, V. Low kinetic inductance superconducting MgB_2 nanowires with a 130 ps relaxation time for single-photon detection applications. *Supercond. Sci. Technol.* **2021**, *34*, 44001. [CrossRef]
13. Ishida, T.; Nishikawa, M.; Fujita, Y.; Okayasu, S.; Katagiri, M.; Satoh, K.; Yotsuya, T.; Shimakage, H.; Miki, S.; Wang, Z.; et al. Superconducting MgB_2 Thin Film Detector for Neutrons. *J. Low Temp. Phys.* **2008**, *151*, 1074. [CrossRef]
14. Kogan, V.G.; Zhelezina, N.V. Penetration-depth anisotropy in two-band superconductors. *Phys. Rev. B* **2004**, *69*, 132506. [CrossRef]
15. Ueda, K.; Naito, M. In Situ growth of superconducting MgB_2 thin films by molecular-beam epitaxy. *J. Appl. Phys.* **2003**, *93*, 2113. [CrossRef]
16. Harada, Y.; Takahashi, T.; Kuroha, M.; Iriuda, H.; Nakanishi, Y.; Izumida, F.; Endo, H.; Yoshizawa, M. Fabrication of as-grown MgB_2 films on ZnO (0001) substrates by molecular beam epitaxy. *Phys. C Supercond. Appl.* **2006**, *445–448*, 884–886. [CrossRef]
17. Shishido, H.; Yoshida, T.; Ishida, T. Ambient temperature epitaxial growth of MgB_2 thin films with a Mg buffer layer. *Appl. Phys. Express* **2015**, *8*, 113101. [CrossRef]
18. Pfaff, C.; Petit-Watelot, S.; Andrieu, S.; Pasquier, L.; Ghanbaja, J.; Mangin, S.; Dumesnil, K.; Hauet, T. Spin injection at MgB_2-superconductor/ferromagnet interface. *Appl. Phys. Lett.* **2024**, *125*, 102601. [CrossRef]
19. Bothner, D.; Gaber, T.; Kemmler, M.; Koelle, D.; Kleiner, R.; Wünsch, S.; Siegel, M. Magnetic hysteresis effects in superconducting coplanar microwave resonators. *Phys. Rev. B* **2012**, *86*, 014517. [CrossRef]
20. Roitman, A.; Shaulov, A.; Yeshurun, Y. Effect of Magnetic Fields on Superconducting Microwave Coplanar Resonators. *IEEE Trans. Appl. Supercond.* **2023**, *33*, 1–4. [CrossRef]
21. Lahl, P.; Wordenweber, R. Nonlinear microwave properties of HTS thin film coplanar devices. *IEEE Trans. Appiled Supercond.* **2003**, *13*, 2917. [CrossRef]
22. Bothner, D.; Clauss, C.; Koroknay, E.; Kemmler, M.; Gaber, T.; Jetter, M.; Scheffler, M.; Michler, P.; Dressel, M.; Koelle, D.; et al. Reducing vortex losses in superconducting microwave resonators with microsphere patterned antidot arrays. *Appl. Phys. Lett.* **2012**, *100*, 12601. [CrossRef]
23. Song, C.; Heitmann, T.W.; DeFeo, M.P.; Yu, K.; McDermott, R.; Neeley, M.; Martinis, J.M.; Plourde, B.L.T. Microwave response of vortices in superconducting thin films of Re and Al. *Phys. Rev. B* **2009**, *79*, 174512. [CrossRef]
24. Rieke, G.H. *Detection of Light: From the Ultraviolet to the Submillimeter*, 2nd ed.; Cambridge University Press: Cambridge, UK, 2003.
25. Mazzocchi, F.; Driessen, E.; Shu, S.; Merker, M.; Ilin, K.; Siegel, M.; Meier, A.; Straus, D.; Scherer, T. Design of NbN Based Kinetic Inductance Detectors for Polarimetric Plasma Diagnostics. *IEEE Trans. Appl. Supercond.* **2021**, *31*, 1–7. [CrossRef]
26. Gao, J. The Physics of Superconducting Microwave Resonators. Ph.D. Thesis, California Institute of Technology, Pasadena, CA, USA, 2008.
27. Askerzade, I.N.; Gencer, A. London penetration depth l(T) in two-band Ginzburg–Landau theory: Application to MgB2. *Solid State Commun.* **2002**, *123*, 63–67. [CrossRef]

28. Larbalestier, D.C.; Cooley, L.D.; Rikel, M.O.; Polyanskii, A.A.; Jiang, J.; Patnaik, S.; Cai, X.Y.; Feldmann, D.M.; Gurevich, A.; Squitieri, A.A.; et al. Strongly linked current flow in polycrystalline forms of the superconductor MgB_2. *Nature* **2001**, *410*, 186. [CrossRef]
29. Ghigo, G.; Botta, D.; Chiodoni, A.; Gozzelino, L.; Gerbaldo, R.; Laviano, F.; Mezzetti, E.; Monticone, E.; Portesi, C. Effective gap at microwave frequencies in MgB_2 thin films with strong interband scattering. *Phys. Rev. B* **2005**, *71*, 214522. [CrossRef]
30. Kim, M.-S.; Skinta, J.A.; Lemberger, T.R.; Kang, W.N.; Kim, H.-J.; Choi, E.-M.; Lee, S.-I. Reflection of a two-gap nature in penetration-depth measurements of MgB_2 film. *Phys. Rev. B* **2002**, *66*, 64511. [CrossRef]
31. Doyle, S. Lumped Element Kinetic Inductance Detectors. Ph.D. Thesis, Cardiff University, Cardiff, UK, 2008.
32. Souma, S.; Machida, Y.; Sato, T.; Takahashi, T.; Matsui, H. The origin of multiple superconducting gaps in MgB_2. *Nature* **2003**, *423*, 65. [CrossRef]
33. Floris, A.; Sanna, A.; Lüders, M.; Profeta, G.; Lathiotakis, N.N.; Marques, M.A.L.; Franchini, C.; Gross, E.K.U.; Continenza, A.; Massidda, S. Superconducting properties of MgB_2 from first principles. *Phys. C Supercond.* **2007**, *456*, 45. [CrossRef]
34. Pimenov, A.; Loidl, A.; Krasnosvobodtsev, S.I. Energy gap and London penetration depth of MgB_2 films determined by microwave resonator measurements. *arXiv* **2001**. [CrossRef]
35. Moshchalkov, V.; Menghini, M.; Nishio, T.; Chen, Q.H.; Silhanek, A.V.; Dao, V.H.; Chibotaru, L.F.; Zhigadlo, N.D.; Karpinski, J. Type-1.5 Superconductivity. *Phys. Rev. Lett.* **2009**, *102*, 117001. [CrossRef] [PubMed]
36. Agassi, Y.D.; Oates, D.E. Theoretical and experimental evidence for a nodal energy gap in MgB_2. *Supercond. Sci. Technol.* **2017**, *30*, 115015. [CrossRef]
37. Eisterer, M. Magnetic properties and critical currents of MgB_2. *Supercond. Sci. Technol.* **2007**, *20*, R47. [CrossRef]
38. Ferrando, V.; Bernini, C.; Manfrinetti, P.; Marré, D.; Putti, M.; Tarantini, C.; Ferdeghini, C. Upper critical fields of MgB_2 thin films. *Phys. C Supercond.* **2004**, *408–410*, 127. [CrossRef]
39. Bud'ko, S.L.; Canfield, P.C. Superconductivity of magnesium diboride. *Phys. C Supercond. Its Appl.* **2015**, *514*, 142. [CrossRef]
40. Pfaff, C.; Courtois, T.; Koblischka, M.R.; Andrieu, S.; Lin, J.-X.; Hehn, M.; Mangin, S.; Dumesnil, K.; Hauet, T. Magnetic moment of thin film superconductors: When thickness matters. *Phys. Rev. B* **2024**, *110*, 94502. [CrossRef]
41. Grissonnanche, G.; Cyr-Choinière, O.; Laliberté, F.; René De Cotret, S.; Juneau-Fecteau, A.; Dufour-Beauséjour, S.; Delage, M.-È.; LeBoeuf, D.; Chang, J.; Ramshaw, B.J.; et al. Direct measurement of the upper critical field in cuprate superconductors. *Nat. Commun.* **2014**, *5*, 3280. [CrossRef]
42. Sekitani, T.; Miura, N.; Ikeda, S.; Matsuda, Y.H.; Shiohara, Y. Upper critical field for optimally-doped $YBa_2Cu_3O_{7-\delta}$. *Phys. B Condens. Matter* **2004**, *346–347*, 319. [CrossRef]
43. Poole, C.P. *Handbook of Superconductivity*; Academic Press: San Diego, CA, USA, 2000.
44. Vissers, M.R.; Hubmayr, J.; Sandberg, M.; Chaudhuri, S.; Bockstiegel, C.; Gao, J. Frequency-tunable superconducting resonators via nonlinear kinetic inductance. *Appl. Phys. Lett.* **2015**, *107*, 62601. [CrossRef]
45. Xu, M.; Han, X.; Fu, W.; Zou, C.-L.; Tang, H.X. Frequency-tunable high-*Q* superconducting resonators via wireless control of nonlinear kinetic inductance. *Appl. Phys. Lett.* **2019**, *114*, 192601. [CrossRef]
46. Zollitsch, C.W.; O'Sullivan, J.; Kennedy, O.; Dold, G.; Morton, J.J.L. Tuning high-Q superconducting resonators by magnetic field reorientation. *AIP Adv.* **2019**, *9*, 125225. [CrossRef]
47. Oates, D.E.; Dionne, G.F. Magnetically tunable superconducting resonators and filters. *IEEE Trans. Appiled Supercond.* **1999**, *9*, 4170. [CrossRef]